Adsorption (2012) 18:381–393
DOI 10.1007/s10450-012-9417-z

Modeling the extra-column volume in a small column setup for bulk gas adsorption

Lisa Joss · Marco Mazzotti

Received: 6 July 2012 / Accepted: 5 September 2012 / Published online: 20 September 2012

Abstract This study aims at highlighting the importance of an accurate characterization of the extra-column volume (ECV) and presents an experimental and computational protocol based on the characterization of the extra-column volume in terms of step-response experiments performed under various flow rates and pressures of 1 bar, 5 bar and 10 bar. The experiments are interpreted by describing the extra-column volume with a compartment model that reflects the geometry of the physical setup and that involves a stagnant zone to account for the non-ideal flow behavior through the piping system. The use of a mathematical model combining the description of the adsorption column and of the ECV can successfully predict experimental CO_2–H_2 breakthrough profiles performed at different pressures on an activated carbon adsorbent. This work shows how the presence of non-negligible extra-column effects can be accounted for, for the determination of adsorption transport parameters.

Keywords Breakthrough experiment · Extra-column effects · Heat- and mass transfer coefficients · Mathematical modeling

Notation

a	Parameter for temperature dependent description of q_s (J/mol)
A	Parameter for temperature dependent description of K (J/mol)
b	Parameter for temperature dependent description of q_s (mol/kg)
B	Parameter for temperature dependent description of K (1/Pa)
c	Fluid phase concentration (mol/m^3)
c_1	Parameter for pressure and flow rate dependent description of f (s/(cm^3 bar))
c_2	Parameter for pressure and flow rate dependent description of f (–)
C_{ads}	Heat capacity of the adsorbed phase (J/(K kg))
C_g	Heat capacity of the gas (J/(m^3 K))
C_g^{mol}	Specific heat capacity of the gas (J/(K mol))
C_s	Heat capacity of the solid (J/(K kg))
C_w	Lumped heat capacity of the wall (J/(m^3 K))
D_c	Micro-pore diffusivity (m^2/s)
D_e	Macro-pore diffusivity (m^2/s)
D_{eff}	Dispersion coefficient in pipes (m^2/s)
D_L	Axial dispersion coefficient (m^2/s)
d_p	Particle diameter (m)
f	Active volume fraction of the tank with stagnant zone (–)
ΔH	Heat of adsorption (J/mol)
h_L	Heat transfer coefficient (lumping fluid + solid phase) (J/(m^2 s K))
h_W	Heat transfer coefficient wall (J/(m^2 s K))
k	Overall mass transfer coefficient (1/s)
k_1	Parameter for velocity dependent description of D_{eff} (m)
k_2	Parameter for velocity dependent description of D_{eff} (m/s^2)
K	Sips equilibrium constant (1/Pa)
K_L	Effective axial thermal conductivity in the fluid phase (J/(m s K))
p	Fluid pressure (Pa)
P_{amb}	Pressure in the ECV downstream of the BPR (Pa)
P_{in}	Pressure in the ECV upstream of the BPR (Pa)
Q_{amb}	Flow rate in the ECV downstream of the BPR (m^3/s)

L. Joss · M. Mazzotti (✉)
Institute of Process Engineering, ETH Zurich, Sonneggstrasse 3, 8092 Zurich, Switzerland
e-mail: marco.mazzotti@ipe.mavt.ethz.ch

Q_{in}	Flow rate in the ECV upstream of the BPR (m^3/s)
Q_{tot}	Flow rate through the ECV (m^3/s)
q	Solid phase concentration (mol/kg)
q^*	Solid phase concentration at equilibrium (mol/kg)
q_{sat}	Solid phase concentration at saturation (mol/kg)
R	Ideal gas constant (J/(K mol))
r_{in}	Inner column radius (m)
r_{out}	Outer column radius (m)
s	Exponent in Sips isotherm (–)
t	Time (s)
T	Temperature (K)
T_w	Wall temperature (K)
T_{amb}	Ambient temperature (K)
u	Superficial gas velocity (m/s)
V_{tot}	Volume of the ECV (m^3)
V_{tank}	Volume of the tank with stagnant zone (m^3)
w_1	Parameter for pressure and flow rate dependent description of λ ($s/(cm^3$ bar))
w_2	Parameter for pressure and flow rate dependent description of λ (–)
y	Mole fraction (–)
z	Space coordinate in axial direction (m)

Greek letters

ε_b	Bed void fraction (–)
ε_t	Overall void fraction (–)
λ	Fraction of the flow mixing between the active and stagnant zones (–)
μ	Dynamic viscosity (Pa s)
ρ	Fluid phase density (kg/m^3)
ρ_b	Bulk density of the packing (kg/m^3)
ρ_p	Particle density (kg/m^3)
χ_{vol}	Volume ratio of the ECV compartments (–)

Sub- and Superscripts

i	Component i
j	Compartment j of the ECV model
S	Stagnant zone

Acronyms

BPR	Back pressure regulator
ECV	Extra-column volume
EOS	Equation of state
MOF	Metal organic framework
MS	Mass spectrometer
PSA	Pressure swing adsorption
TIS	Tank in series
TSA	Temperature swing adsorption
VSA	Vacuum swing adsorption

1 Introduction

Breakthrough experiments are widely performed with the aim of measuring thermodynamic and kinetic properties of adsorption systems and of calibrating mathematical models for process simulations. In recent years, cyclic adsorption processes such as pressure swing adsorption (PSA), vacuum swing adsorption (VSA) or temperature swing adsorption (TSA) have increasingly been considered in the context of CO_2 capture. At the same time novel adsorbent materials such as metal organic frameworks (MOFs), carbon molecular sieves or modified silicas are being continuously developed. These novel nanoporous materials have high potential due to their exceptional adsorption properties and versatility (Choi et al. 2009). A considerable effort is therefore being made in screening novel materials for favorable thermodynamics and kinetics in the context of CO_2 capture. Typically these are produced in the lab as very small particles, and in limited quantities. As a consequence, breakthrough experiments must be carried out in small columns, which suffer from non-negligible extra-column effects due to the large ratio between extra-column volume (ECV) and column volume. In such cases the truly measured response is a combination of the response of the adsorption column and of that of the ECV. The extra-column volume typically consists of a piping system and components such as valves and fittings that are present between the inlet port and the column and between the column outlet and the detector. These extra-column effects have been extensively studied in the case of liquid chromatography by pulse-response techniques (e.g. Delley 1986; Kaltenbrunner et al. 1997; Fountain et al. 2009; Katsuo et al. 2009). Markedly fewer studies are available in the context of gas chromatography or bulk adsorption.

In cases where the adsorption and the extra-column effects can be assumed to be linear, the traditional point-by-point correction procedure can be applied to the combined response in order to obtain the so-called true response of the adsorption column (Guntuka et al. 2008; Rajendran et al. 2008). Therefore the blank response is recorded by performing step response experiments without the adsorption column. Those must be carried out at the same experimental conditions as the breakthrough experiments, i.e. with the adsorption column, and the true response can be obtained by subtracting the blank response point-by-point from the combined response of the entire system. In the case of bulk adsorption experiments performed with the objective of determining dynamic parameters, traditional correction procedures such as the point-by-point correction cannot be applied, because of the important variations in the outlet flow rate and because of significant heat effects due to adsorption. Since extra-column effects contribute to an additional spread of the measured profiles, it is crucial to correctly account for these effects in order to avoid an erroneous interpretation of the breakthrough curves and an inaccurate estimation of the model parameters, particularly transport parameters.

The most popular models to describe the delay and spread due to ECV are the tank in series (TIS) model and

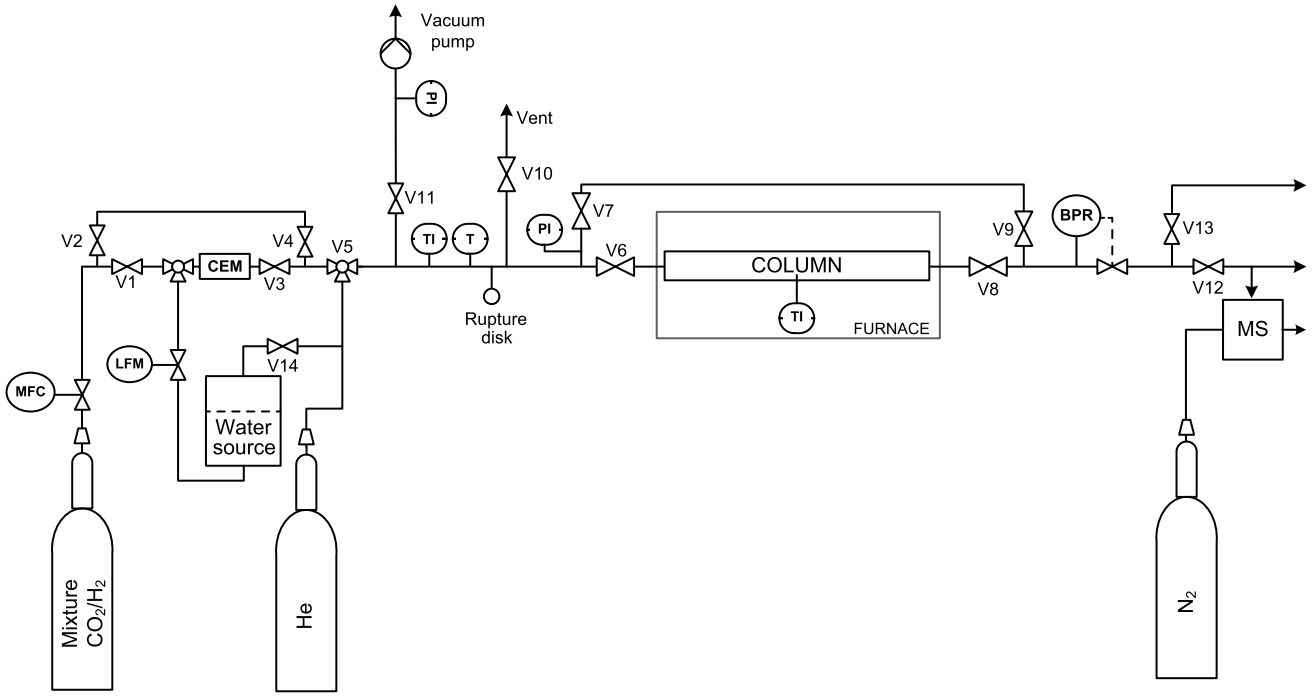

Fig. 1 Flow sheet of the experimental fixed-bed setup

the dispersed plug flow model. Rajendran et al. (2008) developed a correction procedure for extra-column effects in dynamic breakthrough experiments based on the TIS model. The approach adopted in their work was to assume that the true response of the adsorption column can be obtained by the deconvolution of the combined response with the inverse of the TIS model. Dynamic parameters can then be determined by comparing this true response to simulations. In their study only ambient pressure conditions have been considered. However, more complex patterns are observed at higher feed pressures and flow-rates, which cannot be described with simple dispersed plug flow or tanks in series models.

This is the context of this work, whose goal is to develop an experimental and computational protocol and apply it to a significant practical case. Experiments studying the step-response of the piping downstream of the fixed-bed column were performed under a wide range of flow rates and feed pressures up to 10 bar in order to characterize the effect of the ECV of a custom-built small column setup comprised of pipes, valves and a back-pressure regulator. This work highlights the importance of the characterization of the extra-column effects in the context of breakthrough experiments for the estimation of transport parameters, and presents a compartment model able to accurately describe the effect of the extra-column volume under different pressure and flow conditions.

Although this approach has been applied to our specific setup, we believe that it bears general validity in the context of the characterization of small column setups and of their use to estimate transport parameters in adsorption systems.

2 Experimental setup and methods

2.1 Experimental setup

Step response experiments have been performed on the experimental setup shown in Fig. 1. The core of the setup consists of an easily interchangeable stainless steel adsorption column of 0.50 cm diameter and 25 cm length, placed in a Memmert UNE-200 furnace (Schwabach, Germany). The furnace can heat up to a maximum of 300 °C, and the rest of the setup is built to withstand operating conditions of up to 150 °C and 50 bar. Pressure is adjusted with a back pressure regulator (BPR) (EL-LF1, Equilibar, USA) located in the downstream part of the setup. Pressure is recorded with piezo-resistive pressure transmitters (Keller, Jestetten, Germany).

Heating of the pipes is performed with resistive wires; the temperatures of the feed and that inside the column are measured using type K thermocouples (Moser TMT AG, Hombrechtikon, Switzerland). The thermocouple that records the temperature of the fixed bed has a diameter of 0.5 mm and is located at the center of the column, both axially and radially. The feed gas flow is controlled with a mass flow controller (Bronkhorst, Rheinach, Switzerland) operating in the range of 5–250 N ml/min. Gas analysis is performed with

a mass spectrometer (OmniStar, Pfeiffer Vacuum, Switzerland), that cannot be operated above 1 bar.

The volume between the end of the adsorption column and the mass spectrometer (MS) sampling port is referred to as extra-column volume (ECV). It consists of straight and bent piping (0.5 mm inner diameter), fittings, valves and the BPR. Its characterization was done by recording its step response. To this aim the fixed-bed setup was modified by replacing the column with a manual on-off valve (VB) as shown in Fig. 2.

2.2 Materials

The gases used in this study are purchased from Pangas AG (Dagmarsellen, Switzerland). For the ECV step-response experiments N_2 and He at purities of 99.996 % have been used. For the breakthrough experiments a certified binary CO_2–H_2 mixture with a ratio of 1:1 is used. The mixture is produced by Pangas with relative errors of ±0.5 % using the pure gases at purities of 99.995 % for CO_2 and 99.996 % for H_2. A commercial activated carbon adsorbent AP3-60 from Chemviron Carbon (Germany) is used. The original pellets are crushed and sieved in order to obtain 200 µm to 500 µm particles. The adsorbent is regenerated in situ at 150 °C under vacuum for at least 4 hours before the experiments, and a maximum of 4 experiments are carried out before regenerating the adsorbent according to the same procedure. Intermediate regeneration between experiments is performed under milder conditions, namely vacuum for at least 1 hour. The reproducibility of the experiments confirmed that these conditions are sufficient for an effective regeneration of the adsorbent.

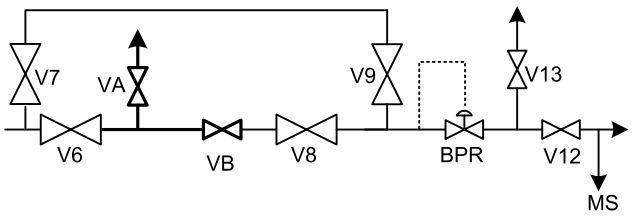

Fig. 2 Modification of the setup by replacing the adsorption column with a manual valve (VB) for the ECV characterization experiments

2.3 Characterization of the extra-column volume

Before each step-response experiment, the ECV is filled with He at the desired pressure. Evacuation of the remaining He upstream of the ECV is carried out under vacuum. A controlled flow rate of N_2 is fed to the ECV and the outlet response is recorded with the MS.

Table 1 summarizes the pressure, temperature and flow conditions of the experiments. Each one was repeated several times, and selected experiments were performed on the non-modified setup using a column with an inert packing, namely glass beads with a diameter of 200 µm to 300 µm.

2.4 Adsorption breakthrough experiments

Breakthrough experiments are performed with the experimental setup shown in Fig. 1 for feed pressures of 1, 5 and

Table 1 Experimental conditions for the different ECV step-response experiments, direct adsorption breakthrough experiments and combined breakthrough experiments

	Experiment	Pressure [bar]	Flow rate [cm^3/s]	Temperature [K]
Extra-column volume	E01-25-a	1.0	0.30	298
	E01-25-b	1.0	0.50	298
	E01-25-c	1.0	0.80	298
	E05-25-a	5.0	0.10	298
	E05-25-b	5.0	0.20	298
	E05-25-c	5.0	0.50	298
	E05-25-d	5.0	1.00	298
	E10-25-a	10.0	0.10	298
	E10-25-b	10.0	0.20	298
	E10-25-c	10.0	0.30	298
	E10-25-d	10.0	0.50	298
Direct breakthrough	D01-25-a	1.0	0.80	298
	D01-25-b	1.0	0.30	298
	D01-25-c	1.0	1.50	298
Combined breakthrough	C01-25	1.0	0.30	298
	C05-25	5.0	0.30	298
	C10-25	10.0	0.30	298

Table 2 Estimated physical characteristics of the setup's components and the matching data of the compartment model. χ_{vol} is the volume ratio of each component with respect to the total ECV volume

	Physical setup		Compartment model		
	Length [cm]	Volume [cm^3]		Length [cm]	χ_{vol} [–]
Piping	19.5	0.25	R1	19.5	0.03
Valve V8	3.0	4.40	R2	–	0.56
Piping	28.5	0.31	R3	30.5	0.18
BPR	2.0	1.10			
BPR	2.0	1.10	R4	23.0	0.23
Piping	8.5	0.06			
Valve V12	2.1	0.20			
Piping	10.4	0.42			

10 bar and at three different flow rates, as listed in Table 1. Additional experiments at 1 bar have also been performed by positioning the MS directly at the column outlet, i.e. between the column outlet and the automatic valve V8. These latter experiments are denominated as *direct breakthrough experiments*.

3 Modeling

3.1 Compartment model of the extra-column volume

Using the dispersed plug flow model or a series of mixed tanks to describe the extra-column volume implies assuming a certain ideal flow behavior. However, deviations from ideal flow may occur by fluid-channeling or the presence of dead or stagnant regions. Compartment models are simple models based on the combination of ideal cases together with dead or stagnant regions (Levenspiel 1999) which have proven to describe non-ideal systems in a satisfactory way (Raghuraman and Varma 1972; Hardin et al. 2001).

The compartment model developed in this work describes the effect of the ECV based on its physical characteristics. The ECV, which is shown in Fig. 2, is schematized as four distinct regions: three pipes with dispersed plug flow, of which two at the feed pressure (R1 and R3) and one at ambient pressure (R4), and a tank (R2). This latter component is composed of an active zone, and of a stagnant zone in which only a fraction of the flow contributes to the mixing. The tank corresponds to the component of the ECV with the largest volume, namely to an automatic valve. The volume ratios of the four different regions (the three pipes and the tank), the lengths of the pipes and the position of the tank and of the BPR are estimated based on the geometry of the different components in the physical setup. Table 2 summarizes what the geometrical characteristics of each component of the ECV are, and how they are accounted for in the model.

The total volume of the ECV can be computed based on step-response experiments performed at 1 bar by considering the average of the measured residence time distribution (RTD). In fact, it can be shown that for an arbitrary reservoir the mean residence time V_{tot}/Q_{tot} is equal to the average of the residence time distribution $E(t)$:

$$t_{mean} = \int_0^\infty t\,E(t)\,\mathrm{d}t = \frac{V_{tot}}{Q_{tot}} \tag{1}$$

where V_{tot} is the volume of the reservoir and Q_{tot} is the flow-rate. For linear systems, the pulse response E is the derivative of the step response F. Equation (1) can therefore be expressed as:

$$t_{mean} = \int_0^\infty t\,\mathrm{d}F = \frac{V_{tot}}{Q_{tot}} \tag{2}$$

This relation can be used to compute the total volume of the reservoir V_{tot} by considering the measured response to a step inlet (F) for a given flow rate Q_{tot}.

Therefore the model parameters that remain to be determined are the volume ratio of the active zone of the tank, f, the ratio of the flow contributing to exchange between the active zone and the stagnant zone of the tank, λ, and the dispersion coefficient in the pipes, D_{eff}. These parameters have been determined by fitting the mathematical model of the extra-column volume to the experimental profiles.

3.1.1 Model equations

The following assumptions are made:

1. the gas phase is ideal,
2. the flow pattern in the pipes can be described by an isothermal dispersed plug flow model,
3. the pressure drop in the single pipes is negligible,
4. the radial dispersion in the pipes is negligible,
5. the expansion is isothermal and isentropic, hence the flow in the low pressure region is determined based on a mass balance.

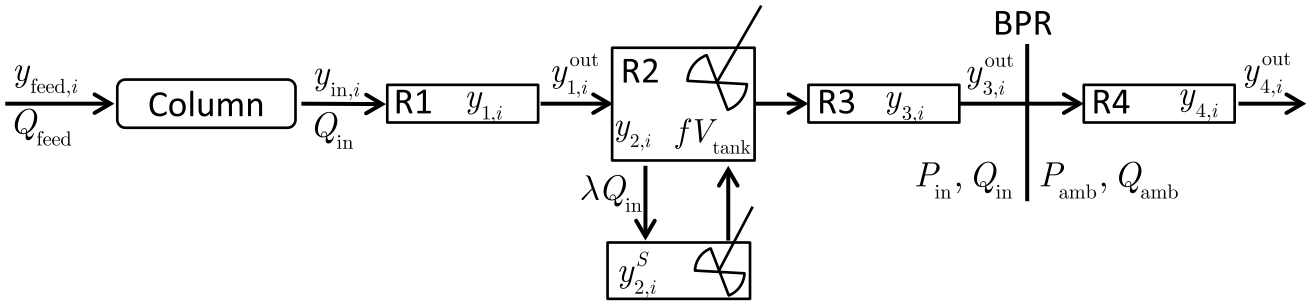

Fig. 3 Schematic representation of the model: adsorption column and extra-column volume. The ECV is subdivided into 4 regions, namely three pipes with dispersed plug flow and one tank with stagnant region. The two pipes downstream of the tank are separated by the back pressure regulator

The tank of volume V_{tank} is subdivided into an active zone and a stagnant zone whose volumes are fV_{tank} and $(1-f)V_{\text{tank}}$, respectively. The mixing flow between the two zones of the tank is a fraction of the total flow through the tank defined as λQ_{tot}. By definition the two parameters f and λ are between 0 and 1. Mass balances over each zone of the tank yields:

$$\left(\frac{V_{\text{tank}}}{Q_{\text{in}}}\right)\frac{\mathrm{d}y_{2,i}}{\mathrm{d}t} = \frac{\lambda}{f}\left(y_{1,i}^{\text{out}} - y_{2,i}\right) + \frac{\lambda}{f}\left(y_{2,i}^{S} - y_{2,i}\right) \tag{3}$$

$$\left(\frac{V_{\text{tank}}}{Q_{\text{in}}}\right)\frac{\mathrm{d}y_{2,i}^{S}}{\mathrm{d}t} = \underbrace{\qquad}_{\text{Active zone}} - \underbrace{\frac{\lambda}{(1-f)}\left(y_{2,i}^{S} - y_{2,i}\right)}_{\text{Stagnant zone}} \tag{4}$$

All the symbols are defined as in the scheme of Fig. 3. The flow in the pipes is described by the convective-dispersive equation, where D_{eff} is an effective axial dispersion coefficient and u is the gas velocity in the pipe ($j = 1, 3, 4$):

$$\frac{\partial y_{j,i}}{\partial t} = -\frac{\partial (u y_{j,i})}{\partial z} + \frac{\partial}{\partial z}\left(D_{\text{eff}}\frac{\partial y_{j,i}}{\partial z}\right) \tag{5}$$

where D_{eff} accounts for molecular diffusion and for turbulent dispersion:

$$D_{\text{eff}} = k_1 + k_2 u \tag{6}$$

Any change in the inlet flow rate Q_{in} is considered to be instantaneously reflected across the entire ECV, and the flow rate in the low pressure region (R4) is determined based on a mass balance over the interface R3–R4:

$$Q_{\text{amb}} = Q_{\text{in}}\frac{P_{\text{in}}}{P_{\text{amb}}} \tag{7}$$

As discussed in Sect. 4.1 the presence of a second mixing mechanism appears clearly in the elution profiles measured at increasing pressure and flow rate. The stagnant region is able to describe this behavior, since the analytical solution of its governing equations ((3) and (4)) consists of the sum of two exponentials. For boundary conditions given as $y_{1,1}^{\text{out}} = 0$ and initial condition $y_{2,1}(t=0) = y_{2,1}^{S}(t=0) = 1$ one obtains:

$$y_{2,1}(t) = g_1\frac{\lambda}{f}\exp(\sigma_1 t) + g_2\frac{\lambda}{f}\exp(\sigma_2 t) \tag{8}$$

$$y_{2,1}^{S}(t) = g_1\left(\frac{1+\lambda}{f} + \sigma_1\right)\exp(\sigma_1 t) + g_2\left(\frac{1+\lambda}{f} + \sigma_2\right)\exp(\sigma_2 t) \tag{9}$$

with:

$$g_i = \frac{(1+\lambda-f) + \sigma_i f(1-f)}{\lambda^2 + \frac{((1-f)(1+\lambda)+f\sigma_i)^2}{f(1-f)}}$$

$$\sigma_1 = \frac{-(1+\lambda-f) + \sqrt{(1+\lambda-f)^2 - 4\lambda f(1-f)}}{2f(1-f)}$$

$$\sigma_2 = \frac{-(1+\lambda-f) - \sqrt{(1+\lambda-f)^2 - 4\lambda f(1-f)}}{2f(1-f)}$$

It can be seen that since $0 \le f, \lambda \le 1$ both σ_1 and σ_2 are negative, and the slower time constant is given by $\tau_1 = -1/\sigma_1$ since $|\sigma_2| > |\sigma_1|$. The presence of the tank with stagnant zone therefore is crucial for an accurate description of the effect of the extra-column volume of this experimental setup.

3.2 Adsorption column

The non-isothermal, non-isobaric one-dimensional adsorption column model used in this work is described in detail by Casas et al. (2012). The governing equations are summarized in Table 3.

The equilibrium adsorbed phase concentration q_i^* is given by a binary Sips adsorption isotherm according to Schell et al. (2011), who studied the same adsorption system CO_2–H_2 on AP3-60 by means of static adsorption measurements over a wide range of pressure and temperature

Table 3 Mathematical model of the adsorption column: mass, energy and momentum balances and equation of state according to (Casas et al. 2012)

Component and total mass balances:

$$\epsilon_t \frac{\partial c_i}{\partial t} + \frac{\partial (u c_i)}{\partial x} + \rho_b \frac{\partial q_i}{\partial t} - \epsilon_t \frac{\partial}{\partial x} - (D_L \frac{\partial c_i}{\partial x}) = 0, \quad i = 1, \ldots, N$$

$$\epsilon_t \frac{\partial c}{\partial t} + \frac{\partial (uc)}{\partial x} + \rho_b \sum_{j=1}^{n} \frac{\partial q_j}{\partial t} = 0$$

Mass transfer (linear driving force)

$$\frac{\partial q_i}{\partial t} = k_i (q_i^* - q_i), \quad i = 1, \ldots, N$$

Energy balance for the fixed-bed:

$$(\epsilon_t C_g + \rho_b C_s + \rho_b C_{\text{ads}}) \frac{\partial T}{\partial t} - \epsilon_t \frac{\partial p}{\partial t} + u C_g \frac{\partial T}{\partial x} - \rho_b \sum_{j=1}^{n} (-\Delta H_j) \frac{\partial q_j}{\partial t} + \frac{2 h_L}{r_i} (T - T_w) - \epsilon_t \frac{\partial}{\partial x} (K_L \frac{\partial T}{\partial x}) = 0$$

Energy balance for the wall:

$$\frac{\partial T_w}{\partial t} = \frac{2\pi}{C_w (r_{\text{out}} - r_{\text{in}})} (r_{\text{in}} h_L (T - T_w) + r_{\text{out}} (T_{\text{amb}} - T_w))$$

Momentum balance (Ergun equation):

$$\frac{\partial p}{\partial x} = -\frac{150 \mu (1-\epsilon_b)^2}{\epsilon_b^3 d_p^2} u - \frac{1.75 (1-\epsilon_b) \rho}{\epsilon_b^3 d_p} |u| u$$

Equation of state (ideal gas law)

$$c_i = \frac{y_i p}{RT}$$

Table 4 Parameters to describe the temperature dependent Sips isotherm (Schell et al. 2011)

			CO_2	H_2
$q_{i,\text{sat}} = a_i \exp(\frac{-b_i}{RT})$	a_i	[mmol/g]	1.38	6.66
	b_i	[J/mol]	−5628	0
$K_i = A_i \exp(\frac{-B_i}{RT})$	A_i	[MPa^{-1}]	1.68×10^{-2}	6.97×10^{-4}
	B_i	[J/mol]	−9159	−9826
$s_i = \alpha_i \text{atan}(\beta_i (T - T_{\text{ref},i})) + s_{\text{ref},i}$	α_i	[−]	0.072	0
	β_i	[K^{-1}]	0.106	0
	$c_{\text{ref},i}$	[−]	0.83	0.96
	$T_{\text{ref},i}$	[K]	329	273

Table 5 Parameters for the adsorption column model

Parameter		Value	
Bulk density of the packing	ρ_b	480	g/cm^3
Particle density	ρ_p	933	kg/m^3
Bed porosity	ϵ_b	0.486	g/cm^3
Particle size	d_p	0.3×10^{-3}	m
Solid heat capacity	C_s	1000	J/K kg
Fluid viscosity	μ	1.4×10^{-5}	kPa s
Isotherm parameters		Table 4	
Heat of adsorption CO_2	ΔH_{CO_2}	−21000	J/mol
Heat of adsorption H_2	ΔH_{H_2}	−9800	J/mol
Heat transfer coefficient	h_L	Table 7	J/K cm^2 s
Mass transfer coefficient	k_i	Table 7	s^{-1}

conditions:

$$q_i^* = q_{i,\text{sat}} \frac{(K_i p_i)^{s_i}}{1 + \sum_{j=1}^{2} (K_i p_i)^{s_i}} \tag{10}$$

where p_i is the partial pressure of component i, $q_{i,\text{sat}}$ and K_i are the saturation capacity and the adsorption equilibrium constant, respectively. The third parameter s_i accounts for the surface inhomogeneity. The temperature dependency of the isotherm parameters is reported in Table 4. The values of the model parameters together with the corresponding sources are listed in Table 5.

3.3 Combined model

The combination of the models presented in Sects. 3.1 and 3.2 is finally used for the prediction of the measured experimental breakthrough profiles on the non-modified setup. Thereby the implicit assumption, which was confirmed by

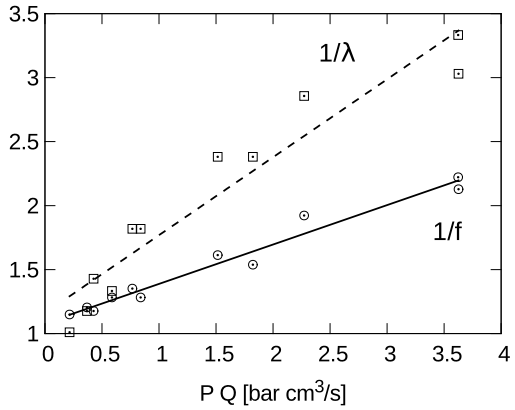

Fig. 4 Values of the reciprocal of the fitted model parameters f (*circles*) and λ (*squares*) as function of the product of the flow rate and feed pressure. Empirical linear dependency $1/f$ (*solid line*) and $1/\lambda$ (*dashed line*)

targeted experiments (see Sect. 4.3), is that the piping upstream of the adsorption column has a negligible contribution to the effective dispersion.

4 Results and discussion

4.1 Characterization of the extra-column volume

The volumes of each region of the compartment model are given by $V_k = \chi_k V_{\text{tot}}$, where χ_k is the estimated volume ratio (cf. Table 2) and V_{tot} is the total extra-column volume. Since the governing equations of the system ((3)–(5)) are linear, (2) can be applied to the step responses performed at ambient pressure to determine the total extra-column volume $V_{\text{tot}} = 9.6\ \text{cm}^3$.

The aforementioned compartment model was fitted to the ECV outlet profiles in order to obtain a set of pressure- and flow-dependent model parameters. To this aim the parameters f and λ, which characterize the tank with stagnant region, were fitted to each experiment independently while keeping the parameters k_1 and k_2, that characterize the effective dispersion in the pipes, constant for all the experiments. It must be noted that the aim of this work is to characterize the effect of the ECV in order to account for it correctly in the description of adsorption breakthrough experiments, and is not to gain a sound understanding of the physics underlying the flow behavior in the piping system. Hence simple empirical relationships for both model parameters as function of the pressure and flow rate are sufficient for this scope. Based on experimental observation, we assume that the reciprocal of f and of λ are linear with respect to the product of the feed pressure times the flow rate, as shown in Fig. 4, where the symbols correspond to the individually fitted parameters, and the solid lines are the following linear regressions:

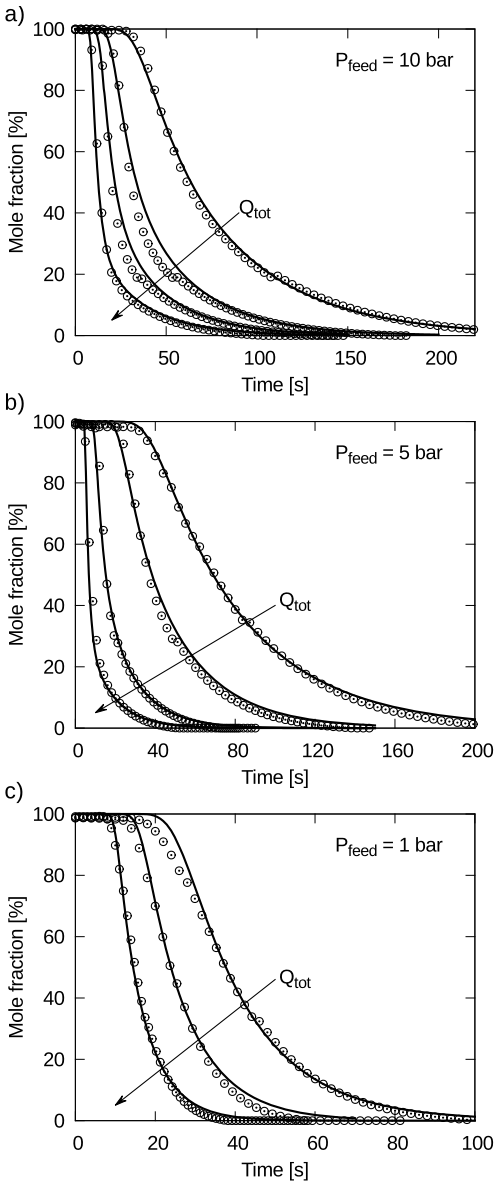

Fig. 5 Outlet profiles of the ECV step response experiments performed for feed pressures of 10 bar (**a**), 5 bar (**b**) and 1 bar (**c**). The *symbols* are the experimental results, the *solid lines* are the simulations of the compartment model with the fitted parameters as in Table 6

$$\frac{1}{f} = c_1 P_{\text{in}} Q_{\text{in}} + c_2 \tag{11}$$

$$\frac{1}{\lambda} = \omega_1 P_{\text{in}} Q_{\text{in}} + \omega_2 \tag{12}$$

Therewith, f and λ can be expressed as function of feed pressure and flow rate with the parameters c_i and ω_i listed in Table 6. Figure 5 shows the experimental ECV outlet profiles together with the simulations performed with the obtained set of pressure- and flow-dependent variables. It is worth noting that the stagnant zone parameters de-

Table 6 Pressure- and flow rate-dependency of the model parameters according to (11) and (12)

c_1 [s/(cm^3 bar)]	c_2 [−]	w_1 [s/(cm^3 bar)]	w_2 [−]	k_1 [m]	k_2 [m/s^2]
0.30	1.08	0.61	1.16	5×10^{-4}	2×10^{-4}

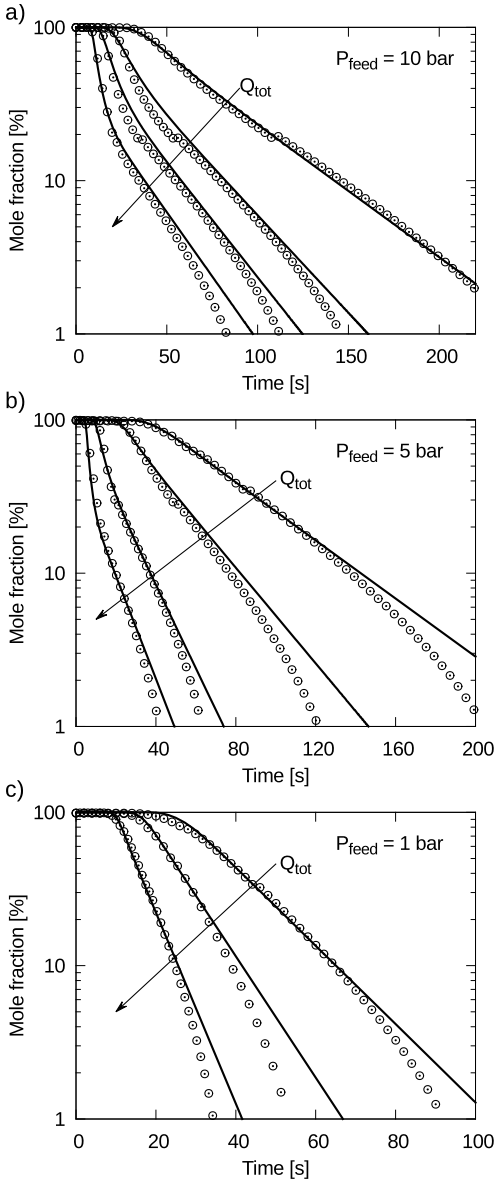

Fig. 6 Semi-log plot of the outlet profiles of the ECV step response experiments performed for feed pressures of 10 bar (**a**), 5 bar (**b**) and 1 bar (**c**). Experimental results (*symbols*) and simulations with the fitted parameters as in Table 6. The appearance of two different slopes for increasing pressure and flow rates indicated the presence of two different mixing mechanisms with different time constants

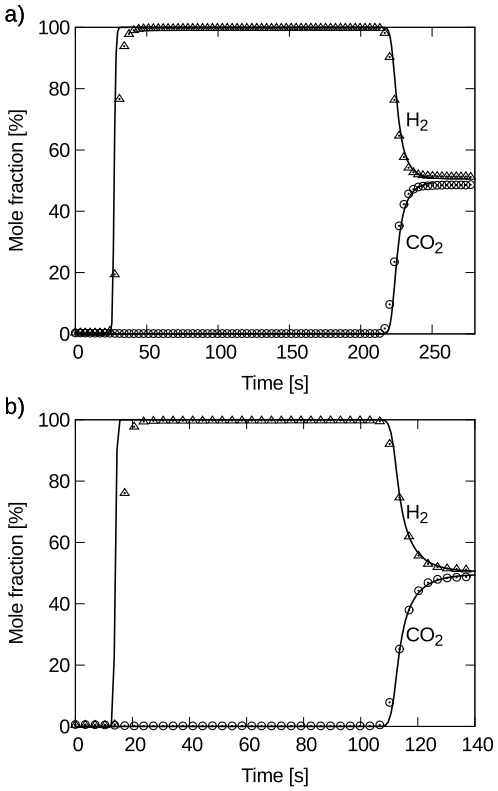

Fig. 7 Outlet profiles for breakthrough experiments recorded directly at the column outlet (*symbols*) and the simulations for which the dynamic parameters h_L, h_W and k_i have been fitted (*solid lines*). (**a**) $Q_{\text{feed}} = 0.3$ cm^3 s^{-1}, (**b**) $Q_{\text{feed}} = 0.8$ cm^3 s^{-1}

Table 7 Heat and mass-transfer coefficients fitted to the experimental breakthrough curves

k_{CO_2} [s^{-1}]	k_{H_2} [s^{-1}]	h_L [J/(m^2 K s)]	h_W [J/(m^2 K s)]
0.53	1.00	200	4.5

pend on the product $P_{\text{in}} Q_{\text{in}}$, which is related to the hydraulic power of the fluid, and not to pressure and flow rate separately; we believe that this is an interesting observation though difficult to explain from a physical point of view.

The chosen set of pressure- and flow rate-dependent variables can describe the response of the ECV to an inlet step successfully in the considered range of operating conditions as shown in Fig. 5. It is worth noting that at higher flow rates and feed pressures the step responses show a rather marked tailing, which results in the appearance of two regions with distinct slopes on a semi-log plot as shown in Fig. 6. The presence of a second distinct slope is characteristic of the presence of a second mixing mechanism with a different time constant, which becomes important only at higher flow rates and pressures.

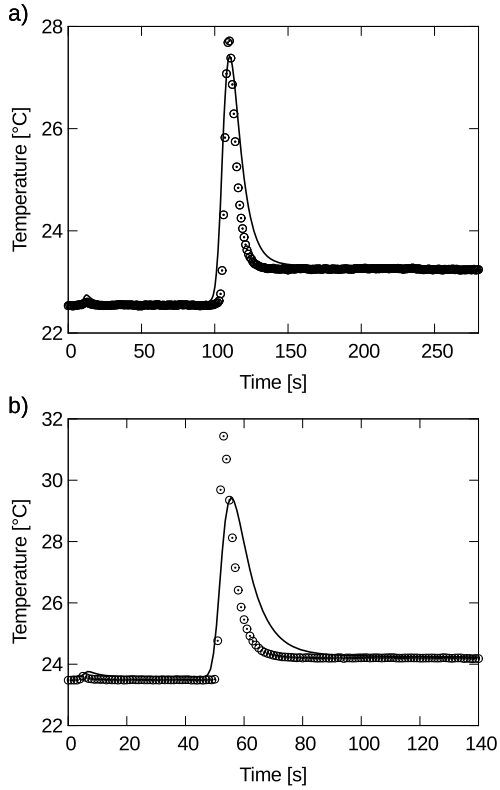

Fig. 8 Temperature profiles at 12.5 cm for breakthrough experiments recorded directly at the column outlet (*symbols*) and the simulations for which the dynamic parameters h_L, h_W and k_i have been fitted (*solid lines*). (**a**) $Q_{\text{feed}} = 0.3\ \text{cm}^3\,\text{s}^{-1}$, (**b**) $Q_{\text{feed}} = 0.8\ \text{cm}^3\,\text{s}^{-1}$

4.2 Adsorption breakthrough experiments

4.2.1 Model validation

The transport parameters of the model, namely the heat transfer coefficients h_L and h_W and the mass transfer coefficients k_{CO_2} and k_{H_2}, have been fitted to the temperature and outlet profiles of breakthrough experiments for which the MS was located directly at the column outlet, hence without any contribution of extra-column effects. The experimental and simulated profiles, for which the heat and mass transfer coefficients have been fitted, are shown in Fig. 7. The corresponding temperature profiles at 12.5 cm are shown in Fig. 8. The values of the fitted transport parameters are listed in Table 7.

4.2.2 Predicting breakthrough curves with the effect of the extra-column volume

The ECV model parameters obtained from the extra-column volume experiments and the heat- and mass-transfer parameters determined from the direct breakthrough experiments were used to predict breakthrough experiments performed with the setup as presented in Fig. 1, i.e. where the effect of the extra-column volume has to be accounted for.

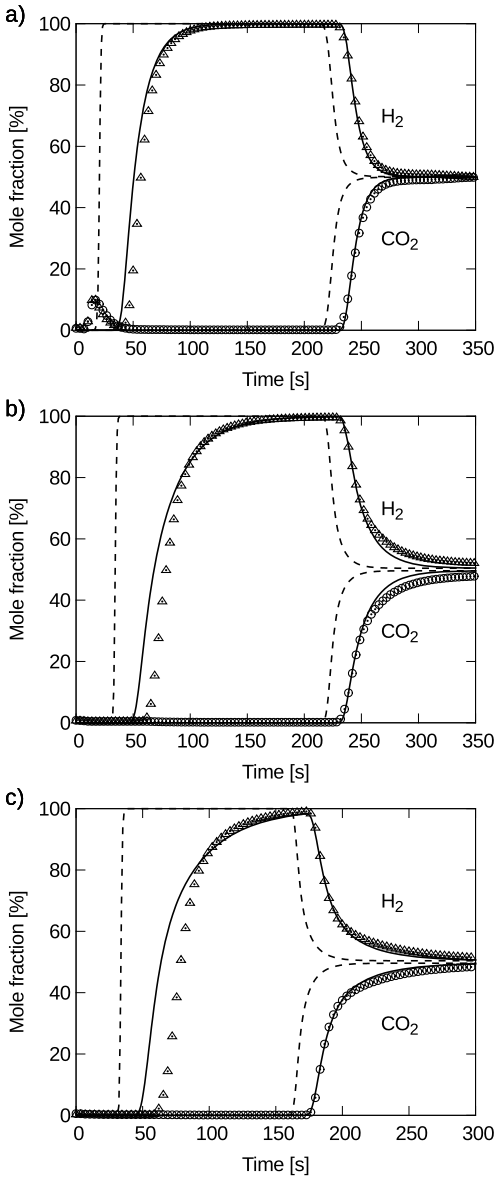

Fig. 9 Outlet profiles for breakthrough experiments recorded downstream of the extra-column volume (*symbols*) and the predicted profiles (*solid lines*). The *dashed lines* are the simulated concentration profiles at the column outlet. (**a**) $P_{\text{feed}} = 1$ bar, (**b**) $P_{\text{feed}} = 5$ bar, (**c**) $P_{\text{feed}} = 10$ bar

In the model it is assumed that the mass transfer coefficient is independent of the velocity and of the feed gas concentration. As discussed in Sect. 4.3, the constant mass transfer rate fitted to the experiments performed at 1 bar is assumed to be applicable also to the breakthrough experiments at higher pressures.

Figure 9 shows the experimental breakthrough profiles and the simulation breakthrough profiles for both the model without ECV (dashed lines) and with ECV (solid lines). It is clear that the combination of the adsorption column model with the extra-column volume compartment model exhibits

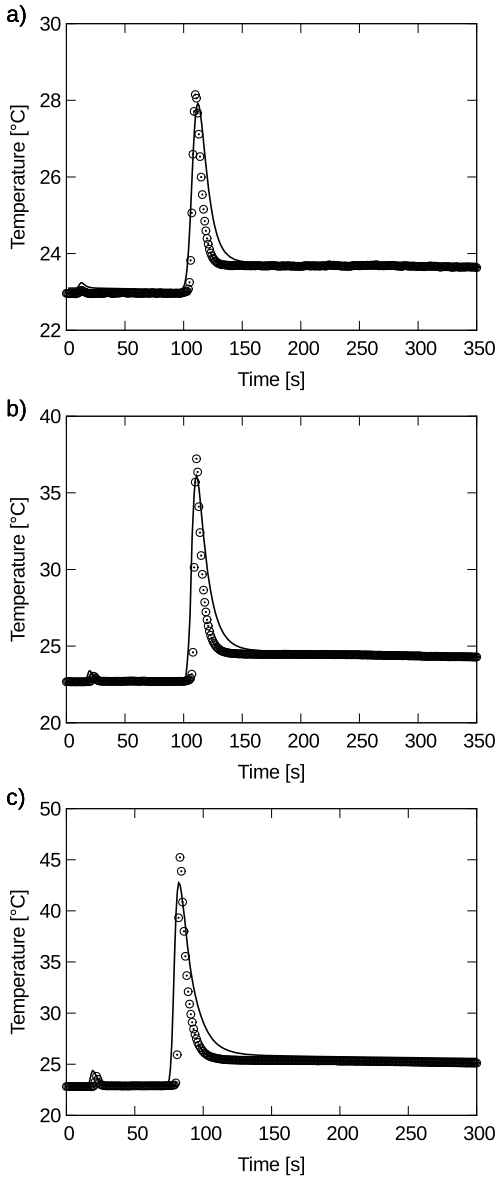

Fig. 10 Temperature profiles at 12.5 cm for breakthrough experiments recorded downstream of the extra-column volume (*symbols*) and the predicted profiles (*solid lines*). (**a**) $P_{\text{feed}} = 1$ bar, (**b**) $P_{\text{feed}} = 5$ bar, (**c**) $P_{\text{feed}} = 10$ bar

a good agreement with the experimental profiles. The temperature profiles corresponding to the simulations are shown in Fig. 10 together with the experimental temperature profiles.

The fully predictive simulations obtained by accounting for the extra-column volume using the compartment model show that an adequate pressure- and flow-dependent characterization of the extra-column effects can be used in combination with the adsorption column model in order to successfully describe and predict experimental breakthrough profiles performed in small column setups with a significant extra-column volume.

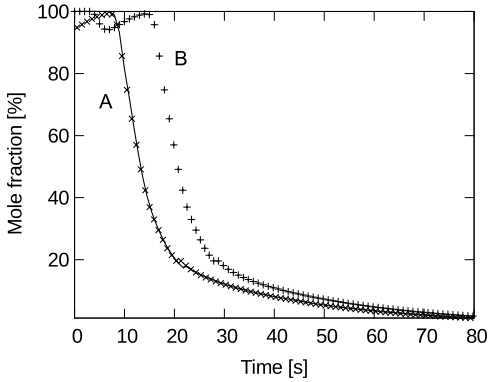

Fig. 11 Step response curves at 10 bar, 0.4 cm^3/s of the setup as shown in Fig. 2 (*curve A*), and of non-modified the setup with an inert column (*curve B*). The *solid line* is obtained by simply shifting the curve B in time

4.3 Validation of the assumptions

In the approach presented in this work to account for extra-column effects, spreading is ascribed solely to the extra-column volume which is downstream of the column. In order to verify this assumption several experiments were performed with the modified setup as illustrated in Fig. 2 as well as with the non-modified setup with a column packed with inert glass beads. Figure 11 shows the step response of the downstream ECV, and that of the entire setup with an inert column for experiments carried out under the same conditions (curves A and B). Both step-responses exhibit an equivalent spreading, the difference in the responses being only a shift in time that stems from the difference in total volume. The solid line is obtained by shifting the response B in time. An overlap with curve A can be observed, which is a clear indication that the mixing in the upstream part of the adsorption column may be neglected.

The predictive simulations shown in Sect. 4.2.2 have been performed by considering a constant mass transfer coefficient that was determined by fitting to experiments performed at 1 bar. It is accepted that for a bi-disperse particle one can distinguish three contributions to the total mass transfer resistance, namely diffusion through the fluid film, macro-pore diffusion and micro-pore diffusion. Haynes and Sarma (1973) showed by means of a moment analysis of the pulse response of a chromatographic column model considering a linear isotherm and external film, macropore and micropore resistances that the resistances are additive and can be combined as follows:

$$\frac{1}{k_i} = \frac{d_p}{6k_{\text{fl}}} H_i + \frac{d_p^2}{60\epsilon_b D_{e,i}} H_i + \frac{r_c^2}{15 D_{c,i}} \tag{13}$$

where k_{fl} is the fluid phase mass transfer coefficient, $D_{e,i}$ the effective macropore diffusivity and $D_{c,i}$ the micro-pore diffusivity. This equation is often referred to as the extended

Glueckhauf approximation. Although this is strictly valid for linear isotherms with a Henry's constant H_i, it is known to provide reasonable estimates for nonlinear systems with H_i replaced by the ratio $q^*_{f,i}/C_{f,i}$ (Hassan et al. 1985; Farooq et al. 2002), where C_f is the feed concentration and $q^*_{f,i}$ is the adsorbed phase concentration in equilibrium with the feed. Assuming a negligible fluid film resistance, there are two contributions to mass transfer resistance in bidisperse particle, namely macro- and micro-pore diffusion. From (13) it can be seen that with decreasing particle size, the macro-pore resistance decreases, hence the micro-pore resistance becomes more important. In the case of activated carbon a critical particle size of $d_p < 1.5$ mm, below which micro-pore resistance is rate limiting, has been suggested by Hu and Do (1993). In this work, all breakthrough experiments have been performed in an adsorption column packed with particles of diameter $d_p = 0.3$ mm, therefore the assumption of negligible macro-pore resistance is reasonable. It follows that the LDF-mass transfer coefficient can be simplified to a single term depending only on micro-pore diffusion:

$$\frac{1}{k_i} = \frac{r_c^2}{15 D_{c,i}} \tag{14}$$

Hence, a micro-pore diffusivity of $D_c/d_c^2 = 3.5 \times 10^{-3}\ \mathrm{s}^{-1}$ is obtained for CO_2 from the fitted mass transfer coefficient. This value is comparable to the values found for CO_2 adsorption on activated carbon, as reported by other researchers. Shen et al. (2010) reported lower micro-pore diffusivities of $D_c/d_c^2 = 1.1 \times 10^{-2}\ \mathrm{s}^{-1}$, and Lopes et al. (2009) found micro-pore diffusivities of $D_c/d_c^2 = 3.35 \times 10^{-2}\ \mathrm{s}^{-1}$ at 303 K. It is worth noting that this is not a true measure of the micropore diffusivity, since the relation between the LDF mass transfer coefficient and the single resistances was developed for isothermal systems with linear isotherms. Nonetheless, it gives a reasonable estimate of the range of micro-pore diffusivity values. From this analysis, the mass transfer coefficient will be expected to depend on the temperature, since micro-pore diffusion is an activated process, but no dependency on the velocity and pressure is expected.

Additional simulations have been performed to assess the possibility of simplifying the proposed model, i.e. by considering a simpler compartment model, as used by Casas et al. (2012) for the description of CO_2–H_2 fixed bed experiments performed in a larger setup. Plug flow through two isothermal pipes at different pressure is considered, and the volumetric flow variation due to the pressure change is accounted for by a mass balance. Figure 12 shows the experimental profile for a breakthrough experiment performed at 10 bar, 0.4 cm^3/s in comparison to a simulated profile for which the simpler plug flow model was used to describe the effect of the ECV. The heat and mass transfer coefficients

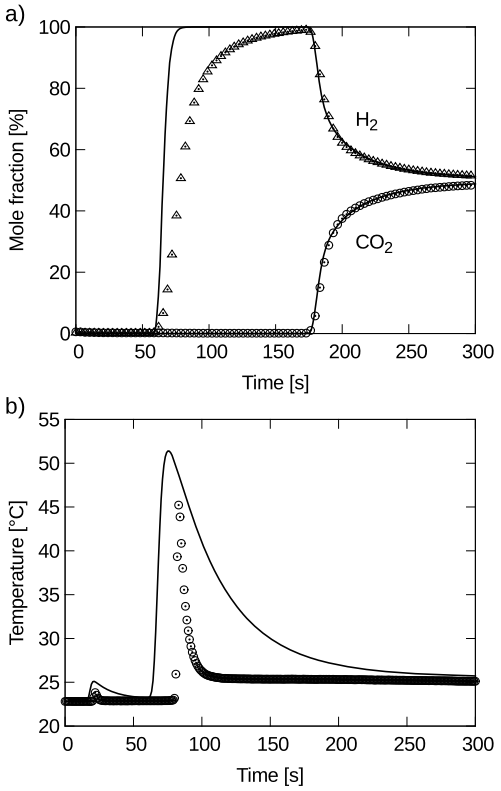

Fig. 12 Outlet (**a**) and temperature (**b**) profiles for a breakthrough experiment performed at 10 bar (*symbols*). Comparison to simulations considering a simple extra-column volume correction procedure (*solid lines*)

have been fitted to the CO_2 front of the concentration profile. An accurate description of the CO_2 front can be achieved by choosing a heat transfer coefficient $h_L = 41\ \mathrm{J\,m^{-2}\,s^{-1}\,K^{-1}}$ and a mass transfer coefficient $k_{CO_2} = 0.25\ \mathrm{s}^{-1}$. These values do not agree with the fitted heat and mass transfer coefficients of the model considering the description of the ECV including the tank with stagnant zone. It is clear that the use of the simpler ECV model leads to an erroneous estimation of the CO_2 mass transfer resistance and of the heat transfer in the packed bed. In fact the corresponding simulated temperature profiles do not match the experimental ones. This shows that the use of a more complex model for small column setups is necessary for an accurate estimation of the dynamic adsorption parameters.

5 Conclusions

The extra-column effects in a small column setup for bulk gas adsorption have been studied under a wide range of pressures and flow-rates. In the case of the investigated setup, the extra-column spreading could be entirely attributed to the downstream extra-column volume. It was shown that deficiencies in the description of the extra-column effects

can lead to erroneous estimates of the adsorption transport parameters, i.e. the heat and mass transfer coefficients. A methodological characterization of the ECV is therefore crucial for the estimation of adsorption transport parameters from breakthrough profiles.

We show how an appropriate compartment model based on the geometrical characteristics of the ECV can be developed and implemented to account accurately for extra-column effects in the evaluation of breakthrough experiments. In the case of our small column setup, more complex patterns that can be described as two mixing mechanisms with different time constants are observed. This can be explained by the presence of a stagnant region in the components of the piping system that have a large volume as compared to the total extra-column volume. Calibration of the model parameters is performed with a series of step response experiments considering only the extra-column volume.

The proposed approach is validated by successfully predicting the experimental outlet concentration profiles and fixed-bed temperature profiles of CO_2–H_2 breakthrough experiments on activated carbon. Therefore the transport parameters, that have been determined by means of breakthrough experiments performed at ambient pressure with no extra-column volume, were used together with the known equilibrium adsorption data in a mathematical model of the adsorption column combined with the ECV model. The good agreement of these fully predictive simulations with the experimental data confirms the validity of the suggested method.

An alternative approach to the physical model is the well-known transfer function model as described for the case of chromatography (e.g. Delley 1986; Kaltenbrunner et al. 1997). Such an approach to characterize the ECV can also be considered in the methodology presented in this work, and could be better suited as compared to a physical model for complex piping systems. However, a physical model will typically have fewer parameters in addition to being an advantage per se.

References

Casas, N., Schell, J., Pini, R., Mazzotti, M.: Fixed bed adsorption of CO_2/H_2 mixtures on activated carbon: experiments and modeling. Adsorption (2012). doi:10.1007/s10450-012-9389-z

Choi, S., Drese, J.H., Jones, C.W.: Adsorbent materials for carbon dioxide capture from large anthropogenic point sources. ChemSusChem **2**(9), 796–854 (2009)

Delley, R.: Modifying the Gaussian peak shape with more than one time constant. Anal. Chem. **58**(11), 2344–2346 (1986)

Farooq, S., Qinglin, H., Karimi, I.: Identification of transport mechanism in adsorbent micropores from column dynamics. Ind. Eng. Chem. Res. **41**(5), 1098–1106 (2002)

Fountain, K.J., Neue, U.D., Grumbach, E.S., Diehl, D.M.: Effects of extra-column band spreading, liquid chromatography system operating pressure, and column temperature on the performance of sub-2-μm porous particles. J. Chromatogr. A **1216**(32), 5979–5988 (2009)

Guntuka, S., Farooq, S., Rajendran, A.: A- and B-site substituted lanthanum cobaltite perovskite as high temperature oxygen sorbent. 2. Column dynamics study. Ind. Eng. Chem. Res. **47**(1), 163–170 (2008)

Hardin, M.T., Howes, T., Mitchell, D.A.: Residence time distributions of gas drum bioreactors. Biotechnol. Bioeng. **74**(2), 145–153 (2001)

Hassan, M.M., Raghavan, N.S., Ruthven, D.M., Boniface, H.A.: Pressure swing adsorption. II. Experimental study of a nonlinear trance component isothermal system. AIChE J. **31**(12), 2008–2016 (1985)

Haynes, H.W., Sarma, P.N.: A model for the application of gas chromatography to measurements of diffusion in bidisperse structured catalysts. AIChE J. **19**(5), 1043–1046 (1973)

Hu, X., Do, D.D.: Multicomponent adsorption kinetics of hydrocarbons onto activated carbon: Contribution of micropore resistance. Chem. Eng. Sci. **48**(7), 1317–1323 (1993)

Kaltenbrunner, O., Alois, J., Yamamoto, S.: Prediction of the preparative chromatography performance with a very small column. J. Chromatogr. A **760**(1), 41–53 (1997)

Katsuo, S., Langel, C., Schanen, P., Mazzotti, M.: Extra-column dead volume in simulated moving bed separations: theory and experiments. J. Chromatogr. A **1216**(7), 1084–1093 (2009)

Levenspiel, O.: Chemical Reaction Engineering, 3rd edn. Wiley, New York (1999)

Lopes, F.V.S., Grande, C.A., Ribeiro, A.M., Loureiro, J.M., Evaggelos, O., Nikolakis, V., Rodrigues, A.E.: Adsorption of H_2, CO_2, CH_4, CO, N_2 and H_2O in activated carbon and zeolite for hydrogen production. Sep. Sci. Technol. **44**(5), 1045–1073 (2009)

Raghuraman, J., Varma, Y.B.G.: A model for residence time distribution in multistage systems with cross-flow between active and dead regions. Chem. Eng. Sci. **28**, 585–591 (1972)

Rajendran, A., Kariwala, V., Farooq, S.: Correction procedures for extra-column effects in dynamic column breakthrough experiments. Chem. Eng. Sci. **63**(10), 2696–2706 (2008)

Schell, J., Casas, N., Pini, R., Mazzotti, M.: Pure and binary adsorption of CO_2, H_2, and N_2 on activated carbon. Adsorption **18**(1), 49–65 (2011)

Shen, C., Grande, C.A., Li, P., Yu, J., Rodrigues, A.E.: Adsorption equilibria and kinetics of CO_2 and N_2 on activated carbon beads. Chem. Eng. J. **160**(2), 398–407 (2010)